Chinese Chemical Letters 35 (2024) 108695

Contents lists available at ScienceDirect

Chinese Chemical Letters

journal homepage: www.elsevier.com/locate/cclet

Resolving the geometric structure of trastuzumab by mobility capillary electrophoresis and native mass spectrometry

Wenjing Zhang, Jie Hong, Lei Yang, Zuqiang Xu, Yu Xiang, Wei Xu*

School of Life Science· Beijing Institute of Technology, Beijing 100081, China

ARTICLE INFO

Article history:
Received 18 February 2023
Revised 25 May 2023
Accepted 15 June 2023
Available online 16 June 2023

Keywords:
Native mass spectrometry
Mobility capillary electrophoresis
Trastuzumab
Protein structure
Geometric structure

ABSTRACT

Available online Immunoglobulins G (IgGs) are Y-shaped globular proteins, however, their high flexibility and heterogeneity pose great challenges to their structure and conformation determinations. Geometric structure of IgG closely correlates to its biofunctions, such as the antibody escape of human immunodeficiency virus (HIV) could attribute to the distance mismatch between the ends of two Fab arms (antigen-binding sites) and envelope glycoprotein spikes on virion surface. Herein, we report the first use of mobility capillary electrophoresis (MCE) and native mass spectrometry (nMS) to resolve the internal geometric structure and conformation of an IgG (trastuzumab) in solution phase. After proteolysis, the ellipsoid dimensions of IgG and its subunits were measured by MCE-nMS experiments. IgG was then reconstructed, in which the sizes and relative positions of these three subunits in three-dimensional space were characterized. It was found that the two Fab arms have an angle of ~102.1° and a distance of ~11.0 nm between the two antigen-binding sites under native condition, and the Fc arm was tilted ~16.0° towards one of the Fab arms. Fc was not on the plane of Fab-Fab, but has an angle of no larger than 103.1°. Under acidic environment (pH 3.0), each subunit of the IgG would unfold into larger dimensions, and the angles between these subunits also change. With great potential for tumor imaging and therapy, the structure of $F(ab')_2$ fragments was also measured and validated by molecular dynamic simulation. It was found that the electrostatic force among these three subunits and steric hindrance stemming from Fc help maintaining the angle between two Fab arms.

IgG proteins are the most abundant type of antibody that protect us against infections by binding antigens with high specificity and affinity [1]. IgG has two antigen binding fragments (Fab) and a crystallizable fragment (Fc) which are connected by the hinge region [2–5]. Generally, these three fragments (or subunits) form a Y-shaped structure [6]. To bind with the vast variety of antigens, IgG is highly flexible in terms of structures [7]. Moreover, post-translational modifications (PTMs) of IgG resulted in molecular heterogeneity and structural complexity [8]. As a result, only a few intact IgG crystal structures have been solved up to date [9–13]. Based on small-angle X-ray scattering measurements and hydrodynamic studies, the crystallohydrodynamic approach has been used to describe IgG solution conformations [14–16]. Even with these advances, it is still challenging to rapidly resolve IgG high resolution structures. Since IgG structure and bioactivity are highly correlated, it is essential to develop relatively efficient methods to resolve the structure and differentiate the conformations of immunoglobulin proteins.

Owing to its high selectivity, specificity and sensitivity, mass spectrometry (MS) has been widely used in proteomics for large scale protein analysis. However, conventional MS technique has limited capability in terms of protein higher-order structure determination [17–22]. Native mass spectrometry (nMS) has emerged as a direct and rapid approach for studying intact proteins and protein complexes [23–26], especially native top-down approach was becoming a hot topic for probing higher-order structure of proteins [27–29]. MS has been further coupled with techniques such as ion mobility (IM), hydrogen/deuterium-exchange (HDX) and chemical cross linking for probing the tertiary and quaternary structures of proteins [30–32]. For instance, IM-MS has been coupled with molecular modeling simulations to study the conformational dynamics of human IgG antibodies during the electrospray ionization process [33–35]. IM-MS and HDX-MS approaches were combined to investigate the thermal unfolding transition characteristics of IgG [36]. The three-dimensional (3D) structural changes of therapeutic mAbs when exposed to degrading conditions were investigated through diethylpyrocarbonate (DEPC) labeling [37]. The application of subzero temperature liquid chromatography (LC) system with amide hydrogen/deuterium exchange-electron

* Corresponding author.
E-mail address: weixu@bit.edu.cn (W. Xu).

https://doi.org/10.1016/j.cclet.2023.108695
1001-8417/

capture dissociation (HDX-ECD) has been used to explore structural changes of therapeutic antibodies (Herceptin) [38,39]. The proposed surface-induced dissociation (SID) in mass spectrometry coupling with macro-molecular docking simulations have been employed to predicted protein complex quaternary structures, which reflects the native structures of protein complexes in solution [40–42]. Recently, mobility capillary electrophoresis (MCE) was developed in our laboratory to measure protein hydrodynamic radius and effective charge [43]. Furthermore, protein 3D shape and dimensions were acquired based on this MCE-nMS technique [44]. Although MS based technique typically could not provide high-resolution structures as those from nuclear magnetic resonance (NMR) or electron microscope (EM), geometric information also correlates to protein biofunctions. For example, trimeric spikes embedded on virion surface has restricted mobility, and the distance between antigen-binding sites correlated with the neutralization potency of an antibody, suggesting that geometric structure measurement may help elucidating antibody escape mechanism and guide vaccine design [45].

To acquire protein finer structure information, this MCE-nMS method was further developed in this work, and applied to characterize the internal structure and conformation of an IgG protein (trastuzumab). The full-length crystal structure of trastuzumab is yet not available [46]. Here, the geometric structure of trastuzumab in solution phase was characterized based on the MCE-nMS method. Besides its overall shape and dimensions [47], the relative position and orientation of its three subunits (Fab, Fab and Fc) were measured under native and denatured conditions. Results agree well with existing IgG crystal structures [13], as well as those from the crystallohydrodynamic and cryo-electron tomography approaches [14,48]. With high sensitivity, protein coarse grained geometric structure information could be acquired within minutes, which could fill in the gap of other high resolution structural biology techniques.

MCE experiments were performed on Lumex CE system (model Capel 105 M, St. Petersburg, Russia), and nMS experiments were carried out on a Waters Xevo G2-XS Tof mass spectrometer instrument (Waters Corporation, Wilmslow, UK) equipped with a nano-ESI source. IgG powder samples were purified and concentrated using Millipore three times for 10 min at every turn. For native MS experiment, the IgG, its subunits (Fab, $F(ab')_2$ and Fc/2), lysozyme and cytochrome C were dissolved in 100 mmol/L ammonium acetate to a final concentration $\sim$ 67 μmol/L. For denatured MS experiment, using formic acid (0.1%) lowers the pH (pH 3.0).

The specific geometric modeling flow of IgG was illustrated in Fig. S1 (Supporting information). Firstly, IgG was digested and fragmented into Fab and Fc by papain, and Ides was also applied to digest IgG into $F(ab')_2$ and Fc/2. The proteolysis products were concentrated and buffer exchanged using Millipore filter (MWO:10 kDa), and a pH 7 was maintained throughout the process. Next nMS experiments were carried out for these proteolysis products. The separation and purification of proteolysis products for MCE experiment were performed on a ÄKTA pure 25 system equipped with a size exclusion column (Superdex 75 increase 10/300GL) using the disodium hydrogen phosphate-citric acid buffer at pH 7. After that, MCE experiments were carried out for Fab, Fc/2 and intact IgG, respectively. Following the theory and data processing method proposed earlier, MCE experiments were carried out to measure the hydrodynamic radius. Through the native MS experiment, the SASA of the protein was acquired based on its charge state distribution measured in the mass spectrum. A quadratic relationship was found between the SASAs and the semi-major axes (a). By combining MCE and native MS results, the ellipsoid radii (a, b and c) of a target protein could be determined [44]. As shown in Figs. 1a and b, protein SASA and hydrodynamic radius (R_h) were acquired from nMS and MCE experiments, and the ellipsoid radii of Fab, Fc/2 and intact IgG were then obtained: (3.53, 3.07, 2.78) nm, (3.60, 2.95, 2.54) nm and (5.49, 5.05, 4.76) nm. Fig. 1c plots the 3D shapes of intact IgG and its subunits, and these 3D shapes have reasonably good agreements with their corresponding crystal structures. The Fc arm consists of two identical Fc/2 stems aligning parallel to each other along their major axes [49].

As a final step, the geometric structure of IgG was reconstructed from its subunits to obtain the values of (α, β, γ). As shown in Fig. S1b, the longest dimension ($2A$) of intact IgG should equal to the maximum edge length of the triangle pyramid, which could either be the edge connecting Fab-Fab or the edge connecting Fab-Fc. Both possibilities have actually been considered, and it was found that the derivation would have a solution only when the edge connecting Fab-Fab equals to $2A$ (details could be found in the supporting information). Thus, the angle between Fab and Fab is calculated by Eq. 1

$$\alpha = 2\arcsin\left(\frac{A}{2a}\right) \tag{1}$$

Subunits were then projected to the cross-sectional plane perpendicular to the longest axis ($2A$). Since the two Fab arms can rotate around their major axes, the projection area of these two Fab arms was within the range of $\pi ac\cos(\alpha/2)$ to $\pi ab\cos(\alpha/2)$. The projection area of Fc arm on this cross section was $2\pi a'c'\cos(\beta)$. Summation of projected areas of Fab arms and Fc should equal to that of intact IgG, and we would have Eq. 2.

$$\arccos\left(\frac{\pi BC - \pi ac\cos\frac{\alpha}{2}}{2\pi a'c'}\right) \le \beta \le \arccos\left(\frac{\pi BC - \pi ab\cos\frac{\alpha}{2}}{2\pi a'c'}\right) \tag{2}$$

Lastly, the edge connecting Fab and Fc should be no longer than the edge connecting Fab and Fab. Therefore, the angle between Fc and Fab-Fab plane (γ) should also satisfy the following equation (Eq. 3).

$$\sqrt{\left(2a\sin\frac{\alpha}{2} + 2a'\cos(\pi-\gamma)\sin\beta\right)^2 + \left(2a\cos\frac{\alpha}{2} + 2a'\cos(\pi-\gamma)\cos\beta\right)^2 + (2a'\sin(\pi-\gamma))^2} \le 2A \tag{3}$$

Four IgG crystal structures are currently available in the PDB database [10–13]. Despite with these general structures available, structural heterogeneity originated from their high flexibility as well as diverse glycosylation modifications makes it difficult for conventional structure analysis techniques to acquire high-resolution structures of immunoglobulins [33,48]. The method proposed in this study can expose the intrinsic structure of IgG under different conditions and help us further understand its structure-function relationship. Fig. 2a plots the geometric structure obtained for IgG under the native condition, in which $\alpha = 102.1°$, $\beta = 16.0° \pm 3.7°$, and $\gamma \le 103.1°$ First, it should be noticed that due to the structural polydispersity of typical mAb structures, these angles obtained here were the averaged angles of trastuzumab. Second, possible ranges of β and γ were obtained instead of exact values. This was due to the fact that each subunit (Fab and Fc) could also rotate along their long axis. After taking these rotations into account in this work, the three ellipsoid radius values obtained from MCE and nMS experiments could only determine the ranges of β and γ.

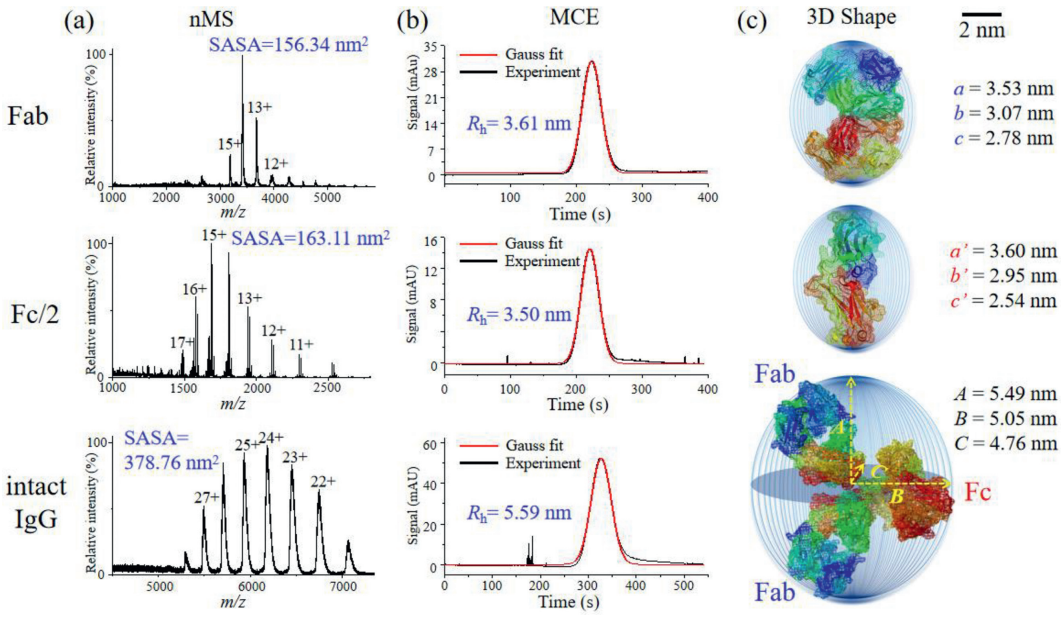

Fig. 1. (a) Native mass spectra of Fab in papain digestion product, Fc/2 in Ides digestion product and intact IgG. (b) MCE experiments of Fab, Fc/2 and intact IgG. (c) The 3D shape and dimensions of Fab, Fc/2 and intact IgG, which were compared with IgG1 crystal structures.

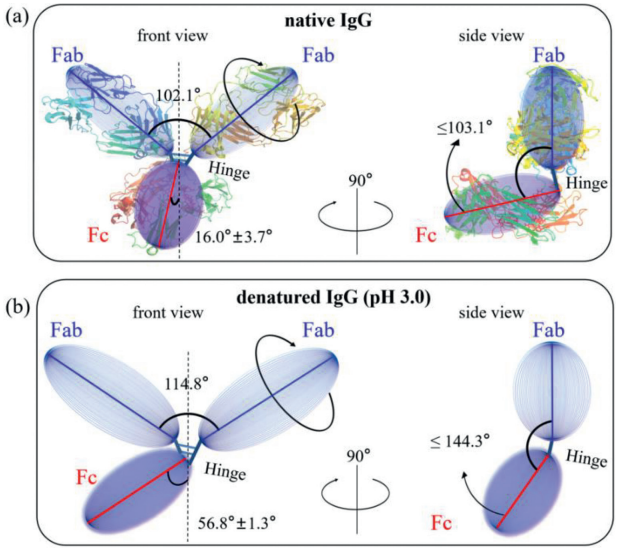

Fig. 2. (a) The resolved geometric structure of IgG (trastuzumab) under native conditions and its comparison with a crystal structure of IgG1 in the PDB database. (b) The resolved geometric structure of IgG (trastuzumab) under denatured condition (pH = 3.0).

Results were compared with an available crystal structure of IgG1 (1IGY) in the PDB database Fig. 2a) [13]. Furthermore, to have a quantitative comparison, these three angles within the crystal structure were calculated based on the centers of gravity of each subunits (details could be found in Supporting information). As a result, α, β and γ calculated within the crystal structure were 98.6°, 21.5° and 100.4°, respectively, which were close (with differences < 6°) to those measured in this work. Results obtained here were further qualitatively compared with those obtained from the crystallohydrodynamic and cryo-electron tomography measurements [14,48]. For instance, using the crystallohydrodynamic method, the angles between Fabs for wild-type, mutant human IgG3s and IgG4s in solution were measured as 80.2°, 108.0° and 122.4°, respectively [14]. Using cryo-electron tomography, the angle between the Fab arms of IgG2a was found to range from 88° to 141° [48]. Both methods also found that Fc was not on the plane of Fab-Fab. The different types of IgG used in these studies would account for the deviations between measurements. Agreement between different methods suggests that the method proposed in this study could be served as an efficient and complement method to probe the structure and conformation of different immunoglobulins under various conditions. Generally, the stability of IgG is a critical property for the development of safe and effective therapeutic protein drugs. Studying the conformational changes as pH change in solution is notoriously difficult since many structural biology methods have limited working parameters. To investigate the conformational change under denatured condition, formic acid (0.1%) was used to lower the solution pH to 3.0 [50]. Similar experiments as those in Fig. 2 were performed to denatured IgG as well as its corresponding subunits (Fig. S3 in Supporting information). At pH 3.0, IgG and its subunits would possess extended conformations, and their ellipsoid radii become: Fab (5.87, 5.30, 4.92) nm, Fc/2 (4.51, 3.84, 3.42) nm and intact IgG (9.89, 6.51, 5.08) nm. After applying the same reconstruction procedure (Eqs. 1-3), it was found that the relative spatial arrangement of these subunits within IgG also changes. The Fab arms would spread away from each other with the angle (α) increase from 102.1° to 114.8° As shown in Fig. 2b, the averaged value of angle (β) changes from 16.0° to 56.8°, indicating that the Fc arm would bend further towards the left Fab arm. Furthermore, the maximum value for the angle γ increases from 103.1° to 144.3°, suggesting that Fc also tends to move away from the Fab-Fab plane under this denatured condition. These angles and their standard deviations were also listed in Table S1 (Supporting information).

As described in Fig. 2, the pH variations result in extensive unfolding and denaturation of IgG [51,52]. The variations of α, β and γ, as well as increased *A*, *B* and *C*, indicate that overall conformational changes of IgG happened at pH 3.0. Especially, the relative position and orientation of Fc with respect to the Fab-Fab plane have changed to a large extent, which might affect the binding of immune effector proteins including the Fc gamma receptors (FcgR), neonatal Fc receptor (FcRn) and complement component C1q at acidic pH conditions [53]. Secondly, the ellipsoid dimensions of IgG and its subunits also increase at pH 3.0. The swelling of IgG and

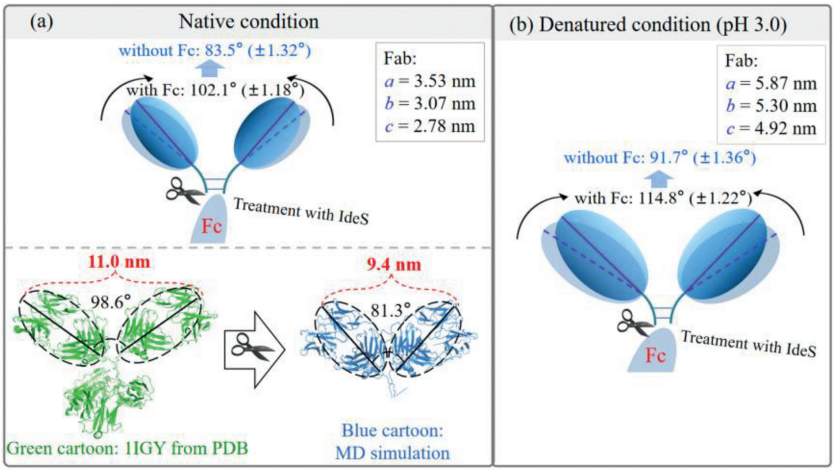

Fig. 3. The geometric structure of F(ab')$_2$ under (a) native condition and (b) denatured condition (pH 3.0). Ellipsoids were experimental results acquired from MCE-nMS. Green cartoon is the PDB structure of an intact IgG (1IGY). Blue cartoon is the F(ab')$_2$ structure from MD simulation.

its subunits would result in the exposure of hydrophobic groups, and cause protein aggregations [54,55]. The antigen binding sites are located on the top of Fab. The geometric expansion of Fab under pH 3.0 indicates that the antigen binding property of this IgG might be altered.

F(ab')$_2$ fragments retain the antigen binding domains of IgG, and they have a specific localizing capability [56]. F(ab′)$_2$ fragments have faster extravasation rates, easier to penetrate into tumor cells and an overall lower residence time of unbound radioimmunoconjugate (RIC) in the body [57–60]. It is suggested that F(ab')$_2$ fragments offer significant promise for tumor imaging and therapy. Next, the structural changes of F(ab')$_2$ compared with intact IgG were explored with the proposed method. As a first step, intact IgG was digested by Ides to obtain the F(ab')$_2$ fragment. Then, MS and MCE experiments were carried out for F(ab')$_2$ fragments under both native and denatured conditions (pH 3.0, Fig. S4 in Supporting information). Following the procedure in Fig. S1c, the ellipsoid dimensions of F(ab')$_2$ and its subunit (Fab obtained from papain digestion) were acquired, and the angles between Fab and Fab were measured. As plotted in Fig. 3a top, the two Fab arms actually get closer to each other (with decreased α angles) without the presence of Fc. Molecular dynamics (MD) simulation was also carried out (Fig. 3a bottom), and the angle (α) obtained from simulation also agrees well with MCE-nMS experiments. Since the ellipsoid shape and dimensions of Fab were not changed under the native condition, the antigen binding capability of each Fab may not be affected [61]. However, the decreased distance between antigen binding sites (from 11.0 nm to 9.4 nm) may prevent F(ab')$_2$ from reaching two antigens spacing further away. Under the denatured low pH condition (pH 3.0), the angle between Fab arms also decrease about 20° by removing the Fc arm (Fig. 3b). Results under both native and denatured conditions show that Fc arm is attracting Fab arms possibility through electrostatic forces, and the presence of Fc would maintain a relatively large spread between these two Fab arms. Besides this angle change, the ellipsoid shape and dimensions of the Fab subunits also expand at pH 3.0, which might be an indicator that the antigen binding functions of F(ab')$_2$ fragments would be affected and modified at this acidic condition [62].

The MCE-nMS method was recently proposed for the overall shape and dimension measurements of proteins. The MCE-nMS based method was further developed for protein internal structure characterization in this study. Specifically, the size, relative position and orientation of trastuzumab's subunits were characterized, and the structures of trastuzumab under native and denatured conditions were reconstructed. Results show that Fc attracts the Fab arms and helps maintaining the spread angle between the two Fab arms, as well as the space between the two antigen binding sites. Acidic environment would cause the conformation change of IgG molecules on two ways: (1) The unfolding of each subunit, which was observed by the increased dimensions of each subunit; (2) the relative position change of its subunits, which was measured by the angle variations. Although finer protein structure information could be acquired compared to our previous study [43,44,63,64], it should be noticed that protein or its subunit geometric structure change is only one type of protein conformation variations. Detailed or localized protein structure changes may not be reflected on its geometric structure. Therefore, protein activity would be affected only when this geometric variation damages its active region.

MCE-nMS offers complementary protein structure information, and it could be incorporated within integrative methodologies. Overall shape and relative position of subunits are complementary to protein information acquired from other methods, such as NMR, HDX, cross-linking and electron microscopy. Therefore, these information could be used as additional restrains to probe protein structure, and combined with other techniques to achieve finer structural analysis. For instance, protein radii have been used to restrain the simulation results from MD simulation to find the most probable conformation of proteins under different conditions [43,44,63,64].

Declaration of competing interest

The authors declare that they have no known competing financial interests or personal relationships that could have appeared to influence the work reported in this paper.

Acknowledgments

This work was supported by Ministry of Science and Technology of the People's Republic of China instrumentation program (No. 2020YFF01014502), NNSFC (No. 21827810) and Beijing Institute of Technology (No. 2021CX006)

Supplementary materials

Supplementary material associated with this article can be found, in the online version, at doi:10.1016/j.cclet.2023.108695.

References

[1] V. Irani, A.J. Guy, D. Andrew, et al., Mol. Immunol. 67 (2015) 171–182.
[2] O.H. Brekke, T.E. Michaelsen, I. Sandlie, Immunol Today 16 (1995) 85–90.
[3] H. Fesseha, T. Degu, D. Endashaw, J. Life Sci. Biomed. 10 (2020) 59–69.
[4] Y. Zhang, F. Shi, C. Zeng, et al., Chin. Chem. Lett. 34 (2023) 107700.
[5] Y. Liu, M. Li, H. Zhu, et al., Chin. Chem. Lett. 32 (2021) 1963–1966.
[6] J. Sha, Z. Ni, L. Liu, H. Yi, Y. Chen, Nanotechnology 22 (2011) 175304–175310.
[7] K.H. Roux, L. Strelets, T.E. Michaelsen, J. Immunol. 159 (1997) 3372–3382.
[8] D. Houde, Y. Peng, S.A. Berkowitz, J.R. Engen, Mol. Cell Proteomics 9 (2010) 1716–1728.
[9] A.M. Davies, B.J. Sutton, Immunol. Rev. 268 (2015) 139–159.
[10] E.O. Saphire, P.W. Parren, R. Pantophlet, et al., Science 293 (2001) 1155–1159.
[11] Y. Wu, A.P. West Jr., H.J. Kim, et al., Cell Rep. 5 (2013) 1443–1455.
[12] L.J. Harris, S.B. Larson, K.W. Hasel, A. McPherson, Biochemistry 36 (1997) 1581–1597.
[13] L.J. Harris, E. Skaletsky, A. McPherson, J. Mol. Biol. 275 (1998) 861–872.
[14] Y. Lu, S.E. Harding, T.E. Michaelsen, et al., Biophys. J. 93 (2007) 3733–3744.
[15] L. Gregory, K.G. Davis, B. Sheth, et al., Mol. Immunol. 24 (1987) 821–829.
[16] W.G. Lilyestrom, S.J. Shire, T.M. Scherer, J. Phys. Chem. B 116 (2012) 9611–9618.
[17] I. Liko, T.M. Allison, J.T.S. Hopper, C.V. Robinson, Curr. Opin. Struct. Biol. 40 (2016) 136–144.
[18] C.V. Robinson, M. Groß, S.J. Eyles, et al., Nature 372 (1994) 646–651.
[19] J. Gault, I. Liko, M. Landreh, et al., Nat. Methods 17 (2020) 505–508.
[20] Z. Su, W. Hu, L. Ye, et al., Chin. Chem. Lett. 34 (2023) 107790.
[21] X. Chang, N. Wang, D. Jiang, et al., Chin. Chem. Lett. 34 (2023) 107522.
[22] Z. Li, Chin. Chem. Lett. 20 (2007) 204–206.
[23] S. Rosati, Y. Yang, A. Barendregt, A.J.R. Heck, Nat. Protoc. 9 (2014) 967–976.
[24] S. Rosati, R.J. Rose, N.J. Thompson, et al., Angew. Chem. Int. Ed. 51 (2012) 12992–12996.
[25] H. Li, H.H. Nguyen, R.R. Ogorzalek Loo, et al., Nature Chem. 10 (2018) 139–148.
[26] Y. Jiang, M. He, W. Zhang, et al., Chin. Chem. Lett. 28 (2017) 1640–1652.
[27] M. Zhou, C. Lantz, K.A. Brown, et al., Chem. Sci. 11 (2020) 12918–12936.
[28] F. Halgand, V. Zabrouskov, S. Bassilian, et al., Anal. Chem. 84 (2012) 4383–4395.
[29] H. Li, J.J. Wolff, S. Orden, J.A. Loo, Anal. Chem. 86 (2013) 317–320.
[30] T.J. El-Baba, D.W. Woodall, S.A. Raab, et al., J. Am. Chem. Soc. 139 (2017) 6306–6309.
[31] G. Wang, I.A. Kaltashov, Anal. Chem. 86 (2014) 7293–7298.
[32] A. Scacioc, C. Schmidt, T. Hofmann, et al., Sci. Rep. 7 (2017) 14008–14022.
[33] K. Hansen, A.M. Lau, K. Giles, et al., Angew. Chem. Int. Ed. 57 (2018) 17194–17199.
[34] K.J. Pacholarz, M. Porrini, R.A. Garlish, et al., Angew. Chem. Int. Ed. 126 (2014) 7899–7903.
[35] K.J. Pacholarz, S.J. Peters, R.A. Garlish, et al., Chembiochem 17 (2015) 46–51.
[36] M.J. Edgeworth, J.J. Phillips, D.C. Lowe, et al., Angew. Chem. Int. Ed. 54 (2015) 15156–15159.
[37] N.B. Borotto, Y. Zhou, S.R. Hollingsworth, et al., Anal. Chem. 87 (2015) 10627–10634.
[38] J. Pan, S. Zhang, C.E. Parker, et al., J. Am. Chem. Soc. 136 (2014) 13065–13071.
[39] H. Gu, G. Dai, S. Liu, et al., Chin. Chem. Lett. 34 (2023) 107715–107719.
[40] A.Q. Stiving, Z.L. VanAernum, F. Busch, et al., Anal. Chem. 91 (2019) 190–209.
[41] J.T. Seffernick, S.R. Harvey, V.H. Wysocki, et al., ACS Cent. Sci. 5 (2019) 1330–1341.
[42] F. Busch, Z. VanAernum, Y. Ju, et al., Anal. Chem. 90 (2018) 12796–12801.
[43] W. Zhang, H. Wu, R. Zhang, et al., Chem. Sci. 10 (2019) 7779–7787.
[44] H. Wu, R. Zhang, W. Zhang, et al., Chem. Sci. 11 (2020) 4758–4765.
[45] J.S. Klein, P.N. Gnanapragasam, R.P. Galimidi, et al., Proc. Natl. Acad. Sci. U. S. A. 106 (2009) 7385–7390.
[46] S. Joshi, L.R. Khatri, A. Kumar, A.S. Rathore, J. Pharm. Biomed. Anal. 195 (2021) 113841–113847.
[47] K. Kühnel, Nat. Chem. Biol. 17 (2021) 626–626.
[48] S. Sandin, L.G. ÖFverstedt, A. Wikström, W. Örjan, U. Skoglund, Structure 12 (2004) 409–415.
[49] D. Moiani, M. Salvalaglio, C. Cavallotti, et al., J. Phys. Chem. B 113 (2009) 16268–16275.
[50] N. Leloup, P. Lössl, D.H. Meijer, M. Brennich, A.J.R. Heck, Nat. Commun. 8 (2017) 1708–1723.
[51] G. Pintér, H. Schwalbe, Angew. Chem. Int. Ed. 59 (2020) 22086–22091.
[52] J. Wirmer, T. Kühn, H. Schwalbe, Angew. Chem. Int. Ed. 40 (2001) 4248–4251.
[53] E. Lopez, N.E. Scott, B.D. Wines, et al., Front. Immunol. 10 (2019) 2415–2429.
[54] R.F. Latypov, S. Hogan, H. Lau, H. Gadgil, D. Liu, J. Biol. Chem. 287 (2012) 1381–1396.
[55] F. Sziegat, J. Wirmer-Bartoschek, H. Schwalbe, Angew. Chem. Int. Ed. 50 (2011) 5514–5518.
[56] S. Hermanto, M. Yusuf, A. Mutalib, S. Hudiyono, J. Phys.: Conf. Ser. 835 (2017) 012005.
[57] K.J. Wong, K.E. Baidoo, T.K. Nayak, et al., EJNMMI Res. 1 (2011) 1–15.
[58] C. Dumolyn, S. Schoonooghe, L. Moerman, et al., EJNMMI Res. 3 (2013) 25–34.
[59] D.M. Lane, K.F. Eagle, R.H. Begent, et al., Br. J. Cancer 70 (1994) 521–525.
[60] F. Buchegger, A. Pèlegrin, N. Hardman, et al., Int. J. Cancer (1992) 416–422.
[61] L.V. Abaturov, R.S. Nezlin, T.I. Vengerova, et al., Biochim. Biophys. Acta 194 (1969) 386–396.
[62] S. Rosenstein, L.Levy A.Vaisman-Mentesh, et al., Curr. Protoc. Mol. Biol. 131 (2020) 119–132.
[63] M. He, P. Luo, J. Hong, et al., ACS Omega 4 (2019) 2377–2386.
[64] W. Zhang, Y. Xiang, W. Xu, TrAC Trends Anal. Chem. 157 (2022) 116739.